COO-2677-12

NOTICE

PORTIONS OF THIS REPORT ARE ILLEGIBLE. It has been reproduced from the best available copy to permit the broadest possible availability.

ADAPTATION OF JET ACCUMULATION TECHNIQUES FOR ENHANCED ROCK CUTTING

by

Dr. Marian Mazurkiewicz
Instytut Technologii Budowy Maszyn
Politechnika Wroclawska - Poland

Dr. Clark R. Barker
Rock Mechanics and Explosives Research Center
University of Missouri-Rolla

Dr. David A. Summers
Rock Mechanics and Explosives Research Center
University of Missouri-Rolla

950 3033

DISCLAIMER

ABSTRACT: The velocity of water jet flow can be increased when the jet impacts a target material or another water jet. A theory describing such augmentation in terms of velocity, mass and energy change is considered. The phenomena is sensitive to jet structure and the jet velocity profile. Jet velocity profiles do not remain constant over great distances from the nozzle, and ultimately disrupt into droplets. Within the droplet the profile is more regular and the velocity constant. The theory is extended to cover this case and experimental evidence of jet augmentation and its effects is presented.

KEY WORDS: impact pressure distribution, fluid jet augmentation, droplet impact, erosion, rock.

INTRODUCTION

The use of high pressure water jets as a cutting tool has, within the last five years, become a commercial reality. The range of application has covered a spectrum from cardboard and wood through coal and rubber to metal.

Research investigators have carried out test programs at pressure levels up to 40,000 bar, well above the 25 to 4 Kbar level of commercially available equipment. Such research has shown that there can, under certain circumstances, be benefits to working at these higher pressures. Equipment for this type of work is, however, generally only of the "one of a kind" research tool variety, and results of test findings at the higher pressure levels have indicated relatively short lives for the generating pressure systems and particularly the nozzles, in which the transition to cutting speed occurs.

Because of the problems associated with creating pressures within a piece of equipment, consideration has turned to the possibility of generating high velocities beyond the nozzle by the use of interacting jets or jet impact on a solid surface.

This approach has already been shown successful in the development of shaped charges, particularly for military applications during the last world war [1-3]. Theoretical and experimental analysis of this phenomenon has shown that directional cumulative jet accelerations to velocities of

the order of 1,000 to 2,500 m/s can be achieved. The velocity achieved is a function of the charge size and the shape and material composition of the liner which, upon collapse, will create the cutting jet.

This paper examines the related field where an augmented velocity jet or "fast jet" is produced by the impact between two identical water jets or of a single water jet with a rigid flat surface. The paper extends the existing theory developed for shaped explosive charges to describe the formation and nature of the secondary water jets formed when two identical jets meet. The secondary jets move in opposing directions along the line bisecting the angle between the original jets. The motion of the secondary jets must satisfy the principles of conservation of mass, energy, and momentum. Calculations are thereupon described which govern the mass and velocity of these secondary jets.

Particular considerations are given to the case where one of the secondary jets is of sufficient velocity to have the capability of cutting a target material.

In the passage of a water jet from the nozzle into a surrounding fluid the effect of the jet of the surrounding fluid is to cause a change in the pressure profile (velocity profile) of the jet (Fig. 1). The initial condition with a constant velocity across the profile changes to a Gaussian distribution with increasing distance from the nozzle as the water on the outside of the core is abraded. Conventional theory on jet impact is based on those portions of the curve where the primary jet still retains a constant velocity across

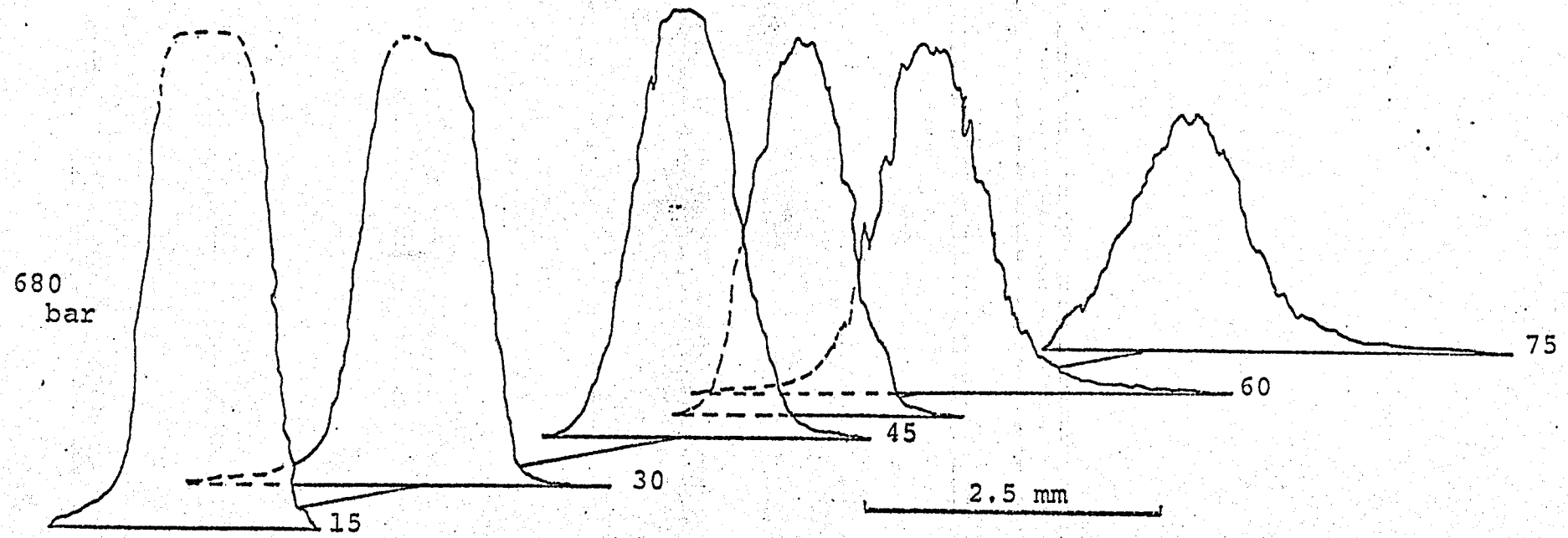

FIG. 1 - Impact pressure profiles at various distances along a water jet issuing from a 1.5 mm nozzle diameter at 545 bar.

the profile, and will then expand this to the case where the jet is broken into droplets.

ANALYTICAL MODEL

Consider an original primary fluid jet in the region close to the nozzle where it retains an even pressure profile across its section. Let such a jet have a square cross-section of area b x b and with a leading edge which is a flat surface. If it is assumed that all portions of the original jet are approaching a rigid flat surface with the same velocity vector inclined at angle α relative to the flat surface and with the leading edge of the primary jet inclined at angle γ to plane A_1A_2. The first portion of the leading edge of the primary jet contacts the plane 00 at point A_1 (Fig. 2). This simulation is equivalent to the intersection of two similar jets approaching a common plane of symmetry 00 at angle γ (Fig. 3).

If the flow were a continuous laminar flow, then the primary jet would divide to produce two streams flowing in opposite directions along the surface 00. Each stream would have a velocity magnitude V_o, where V_o is the magnitude of the inflow velocity. Such a condition is non-typical and a more generalized case will be considered.

Velocity of the Secondary Jets

Sims [4] used a control volume approach to determine the velocity relationship between the primary and secondary jets

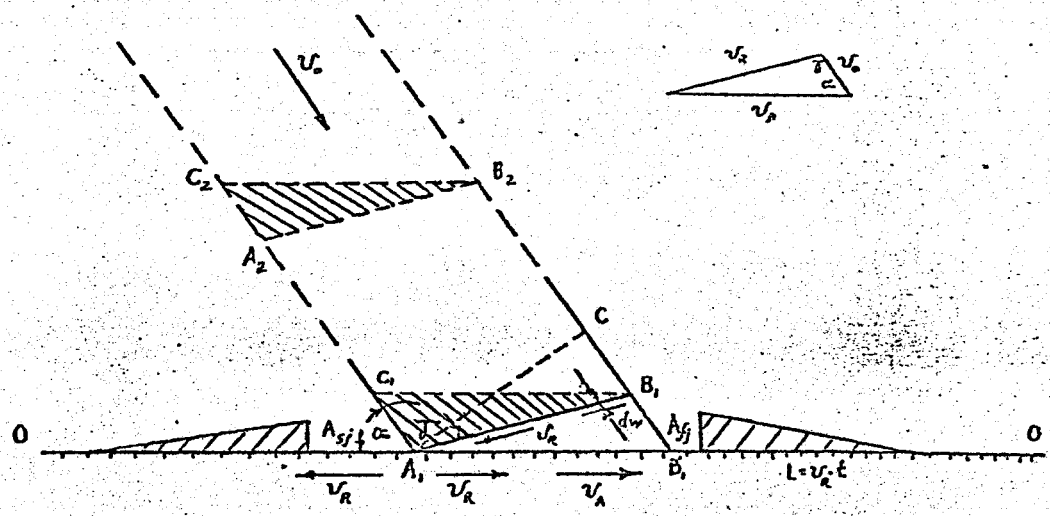

FIG. 2 - Geometric representation of the stages of impact of a flat faced water jet on an oblique plane.

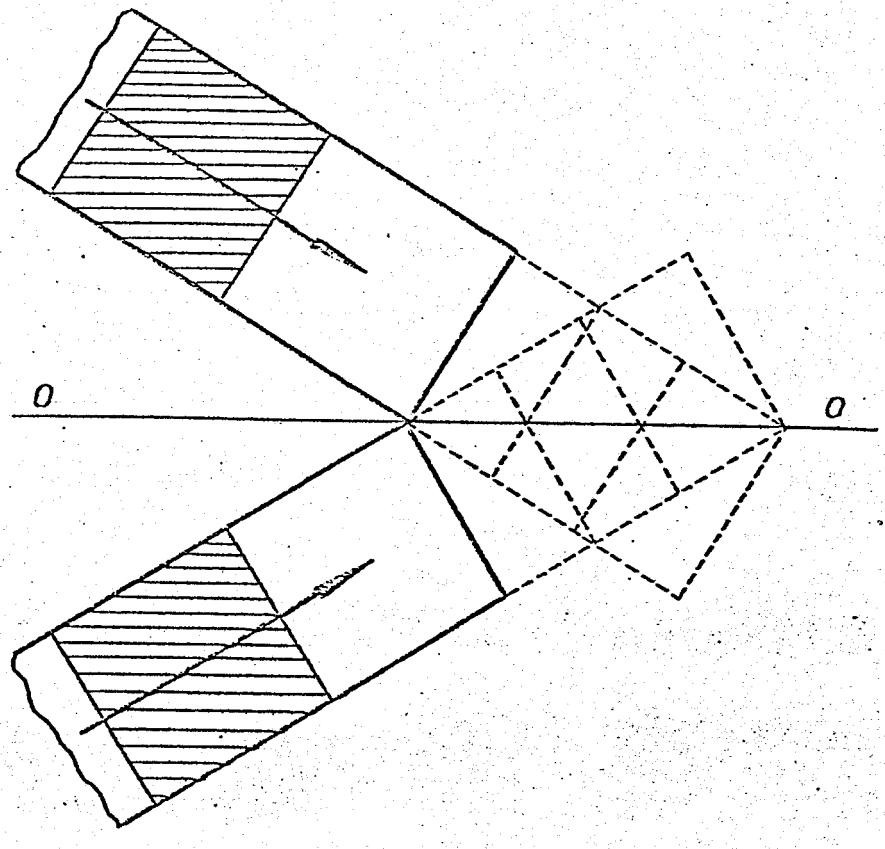

FIG. 3 - Collision of two flat faced square jets.

for the special case $\gamma = 90°$. He concluded that, as the jet contact point A_1 moves along plane 00 at a speed V_A, jets created at the plane would have velocity magnitudes (V_{fj} to the right, herein referred to as the "fast jet", and V_{sj} to the left, herein referred to as the "slow jet") given by the equations

$$V_{fj} = |\bar{V}_R + \bar{V}_A| = V_R + V_A$$

$$V_{sj} = |\bar{V}_A - \bar{V}_R| = V_A - V_R \qquad (1)$$

where V_R is the relative velocity of the primary jet to the jet contact point. From the velocity polygon in Fig. 2 we can derive the following

$$V_R = \frac{V_o \sin\alpha}{\sin(\alpha+\gamma)}$$

$$V_A = \frac{V_o \sin\gamma}{\sin(\alpha+\gamma)} \qquad (2)$$

If Eq 2 is substituted into Eq 1, then

$$V_{fj} = V_o \left[\frac{\sin\alpha + \sin\gamma}{\sin(\alpha+\gamma)}\right] \qquad (3)$$

$$V_{sj} = V_o \left[\frac{\sin\gamma - \sin\alpha}{\sin(\alpha+\gamma)}\right] \qquad (4)$$

Hence, the speed of the secondary jets depends only on V_o, α, and γ.

Mass of the Secondary Jets

The mass of the secondary water jets can be estimated by applying the equations for conservation of momentum and mass at point A_1 (Fig. 2)

$$\int \rho V_R^2 \cos[180° - (\alpha+\gamma)]\, dA_{in} = -\int \rho V_R^2\, dA_{fj} + \int \rho V_R^2\, dA_{sj} \qquad (5)$$

and

$$\int \rho V_R dA_{in} = \int \rho V_R dA_{fj} + \int \rho V_R dA_{sj} \qquad (6)$$

where dA_{in} is the elemental vertical cross section of the inflow jet,

dA_{fj} is the elemental vertical cross section of the fast jet,

dA_{sj} is the elemental vertical cross section of the slow jet.

$$dA_{in} = b\, dw, \qquad (7)$$

$$dw = V_o \sin(180° - \gamma)\, dt$$

substituted into Eqs 5 and 6 gives

$$(A_{fj})_{max} = \int_{o}^{max} dA_{fj} = \frac{b^2[1 + \cos(\alpha+\gamma)] \sin(\alpha+\gamma)}{2 \sin \alpha} \tag{8}$$

$$(A_{sj})_{max} = \int_{o}^{max} dA_{sj} = \frac{b^2[1 - \cos(\alpha+\gamma)] \sin(\alpha+\gamma)}{2 \sin \alpha}$$

The area of the vertical cross section of the secondary water jet impacting on the surface increases linearly from 0 to the value $(A_{fj})_{max}$. This occurs during the time T that point B_1 moves to B_1^1. If we let distance $B_1B_1^1$ be x and consider triangles A_1CB_1 and $A_1B_1B_1^1$, then

$$T = \frac{x}{V_o} = \frac{b \sin(\alpha+\gamma)}{V_o \sin \alpha \sin \gamma} \tag{9}$$

The length of the secondary jet is therefore

$$\ell = V_R T \tag{10}$$

from Eqs 2 and 9 this gives

$$\ell = \frac{b}{\sin \gamma} \tag{11}$$

Secondary jets will have a wedge shape with an area of the base of $(A_{sj})_{max}$ and $(A_{fj})_{max}$, width b, and length ℓ. Letting

the mass density of the water be ρ, the mass of the secondary jets will be

$$(M_{fj})_{max} = \frac{\rho b^3}{4} \frac{[1 + \cos(\alpha+\gamma)]\sin(\alpha+\gamma)}{\sin\alpha \sin\gamma}$$

$$(M_{sj})_{max} = \frac{\rho b^3}{4} \frac{[1 - \cos(\alpha+\gamma)]\sin(\alpha+\gamma)}{\sin\alpha \sin\gamma} \qquad (12)$$

The total mass that participates in the formation of the secondary water jets is the sum of $(M_{fj})_{max}$ plus $(M_{sj})_{max}$,

$$M_{in} = \frac{\rho b^3}{2} \frac{\sin(\alpha+\gamma)}{\sin\alpha \sin\gamma} \qquad (13)$$

Energy of the Secondary Jets

Using Eqs 3, 4, and 12 the kinetic energy of the secondary water jets can be derived

$$EK_{fj} = \frac{\rho b^3 V_o^2}{8} \frac{[1 + \cos(\alpha+\gamma)]\ (\sin\alpha + \sin\gamma)^2}{\sin\alpha \sin\gamma \sin(\alpha+\gamma)}$$

$$EK_{sj} = \frac{\rho b^3 V_o^2}{8} \frac{[1 - \cos(\alpha+\gamma)]\ (\sin\alpha + \sin\gamma)^2}{\sin\alpha \sin\gamma \sin(\alpha+\gamma)} \qquad (14)$$

The kinetic energy of the secondary jets is a function of V_o, b, and angles α and γ.

Concentration of Energy

Even more significant than the energy ratio is the concentration of energy. This information, important in estimating the cutting potential of the secondary jets, is obtained by dividing the kinetic energy by the cross-sectional area of the secondary jets. Hence

$$K_{fj} = \frac{EK_{fj}}{(A_{fj})_{max}} = \frac{\rho b V_o^2}{4} \frac{(\sin \alpha + \sin \gamma)^2}{\sin \gamma \sin^2 (\alpha+\gamma)}$$

$$K_{sj} = \frac{EK_{sj}}{(A_{sj})_{max}} = \frac{\rho b V_o^2}{4} \frac{(\sin \alpha - \sin \gamma)^2}{\sin \gamma \sin^2 (\alpha+\gamma)} \quad (15)$$

The concentration of energy for the primary jet can be written as

$$K_{in} = \frac{EK_{in}}{A_{in}} = \frac{\rho b V_o^2}{4} \frac{\sin^2 (\alpha+\gamma)}{\sin \alpha \sin^2 \gamma} \quad (16)$$

where $A_{in} = b^2$, the area of the cross section of the primary jet. The concentration of energy ratio is then defined as

$$\frac{K_{fj}}{K_{in}} = \frac{(\sin \alpha + \sin \gamma)^2 \sin \alpha}{\sin^3 (\alpha+\gamma)}$$

$$\frac{K_{sj}}{K_{in}} = \frac{(\sin \alpha - \sin \gamma)^2 \sin \alpha}{\sin^3 (\alpha+\gamma)} \quad (17)$$

Analysis of the Theoretical Results

It is obvious from studying the previous equations that the values of α and γ are very important in determining the characteristics of the secondary jets. Fig. 4 was computed for the case $V_o = 1$ and $b = 1$. Note that the actual value of α and γ is not as critical as the sum $(\alpha + \gamma)$. The velocity ratio is high as $(\alpha + \gamma)$ approaches 180 degrees.

The importance of the accumulation phenomena is illustrated by consideration of the pressure (P) that would be required to produce the high velocity ($V = 14\sqrt{P}$) possessed by the secondary water jet if conventional nozzle extrusion methods were used, relative to that of the primary jet stagnation pressure (P_o) where augmentation occurs. If, for example, V is 5051 m/s, then P_o would be 1,000 atm if $\alpha = 80°$ and $\gamma = 90°$. To produce the same velocity with conventional methods would require P to be 65,322 atm.

Fig. 5 is a plot of the kinetic energy ratio EK_{fj}/EK_{in} for various values of α and γ. From this figure it can be seen that the kinetic energy ratio is at a maximum value of 1 when α and γ are equal. Three types of flow can be identified based on the relationship between α and γ (Fig. 5). When $\gamma = \alpha$, all the energy is possessed by the fast secondary jet and the slow jet has none. In the region where $\gamma < \alpha$, the slow secondary jet moves to the left. In the region where $\gamma > \alpha$, the secondary slow jet moves to the right along with the fast secondary jet. Fig. 6 is a plot of the concentration of energy ratio. This figure is very similar to

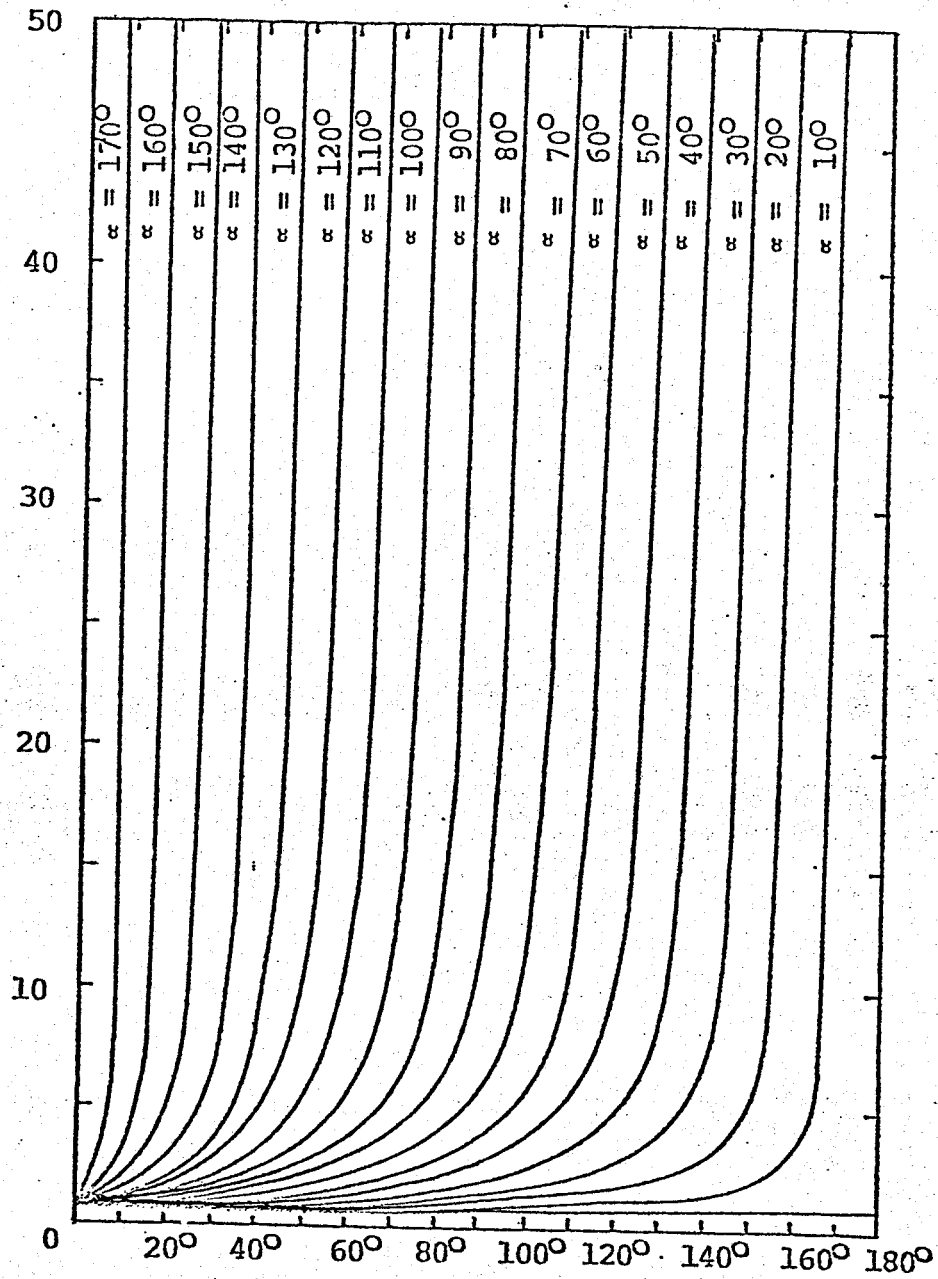

FIG. 4 – Velocity augmentation ratio as a function of the impact angles α and γ.

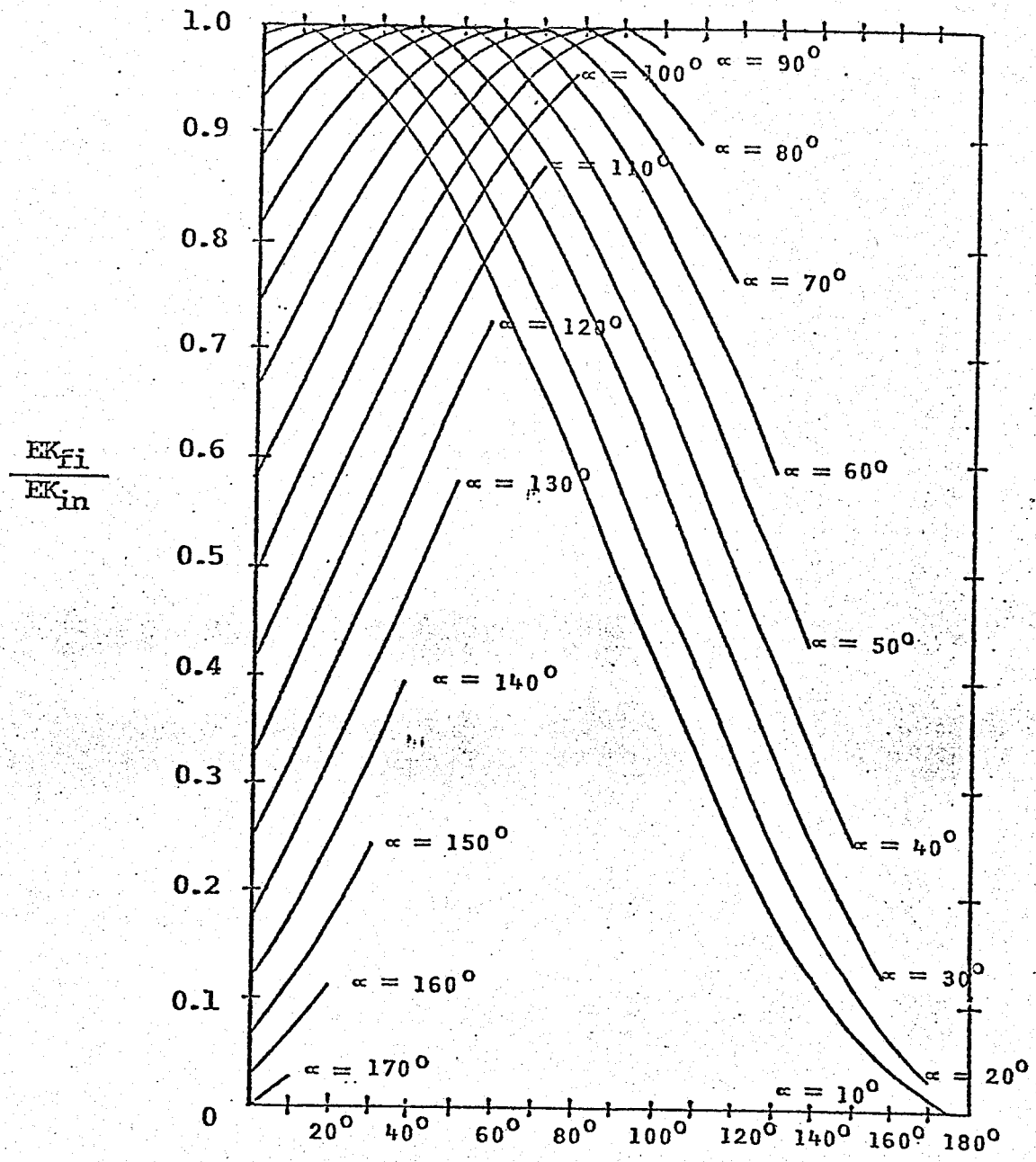

FIG. 5 – Kinetic Energy augmentation ratio as a function of the impact angles α and γ.

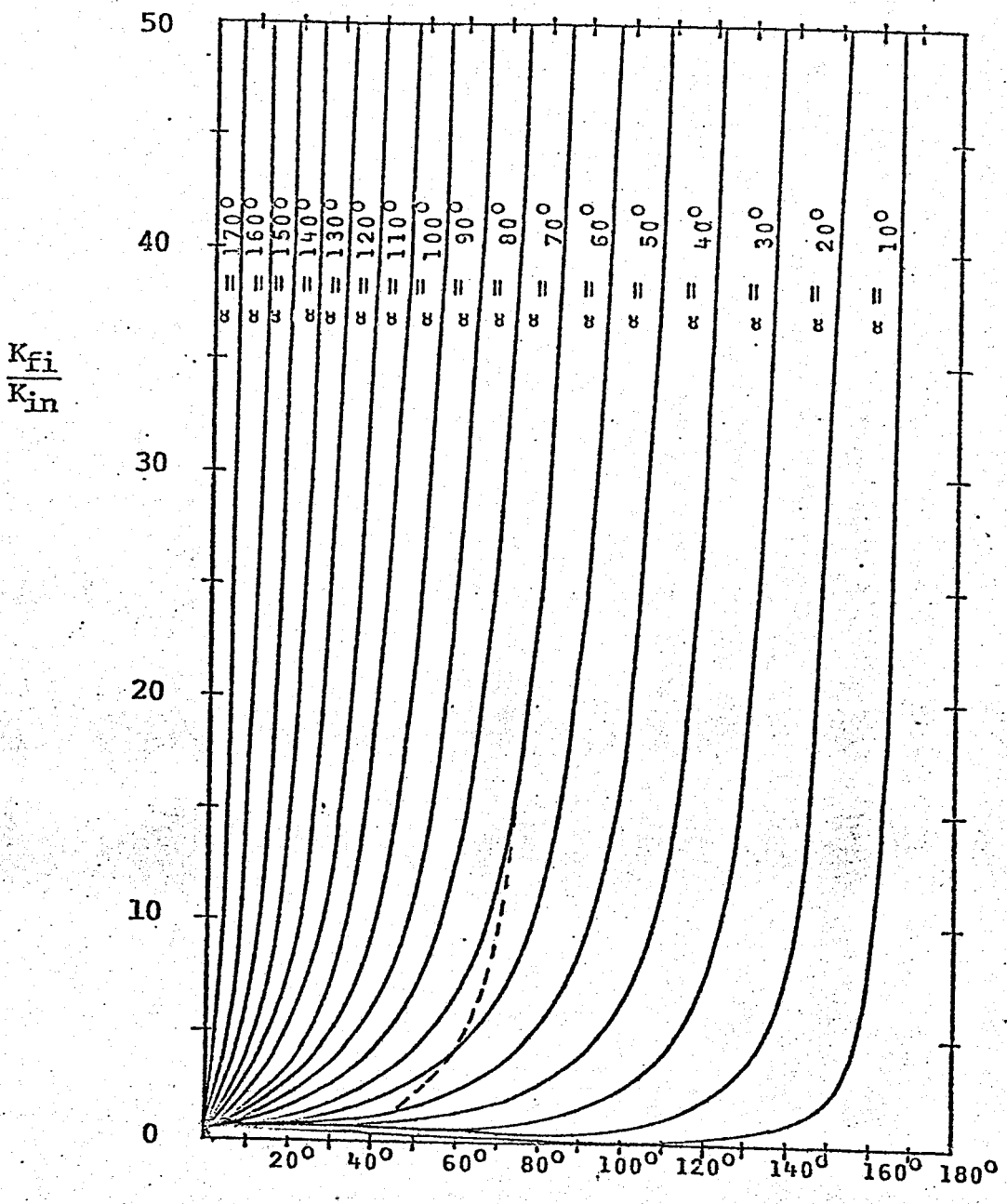

FIG. 6 - Energy intensification ratio as a function of the impact angles α and γ.

Fig. 4 and the same comments apply. Based on the information that the kinetic energy ratio is maximum for $\alpha = \gamma$ (Fig. 5) the optimum condition for energy concentration can be plotted as a dashed line on Fig. 6.

EXPERIMENTAL APPLICATIONS

Under normal circumstances it is extremely difficult to obtain a flat leading edge to a water jet or to maintain a uniform velocity across the jet profile. The surface or profile is generally curved (Fig. 1) or more severly distorted by jet movement relative to the surrounding medium.

However, at the point where the jet breaks into droplets, the contour of the leading surface will stabilize and the velocity will be sensibly constant within the droplet. This set of conditions allows the above analysis to be extended to cover this case. Analysis of this phenomena has been carried out in Cambridge [5] and only a comparative relation will therefore be made.

Fig. 7 shows an element sliced from a spherical droplet, of radius R and moving at speed V_o toward the flat surface 00 at an angle α. Every phase of the collision can be considered using the previously derived equations with suitable transformations to adapt them to the present geometry. For example, when the face of the element from M' to M_1'' contacts the flat surface, the geometry is the same as that of Fig. 2. The droplet first contacts the plane 00 at M_1 and during

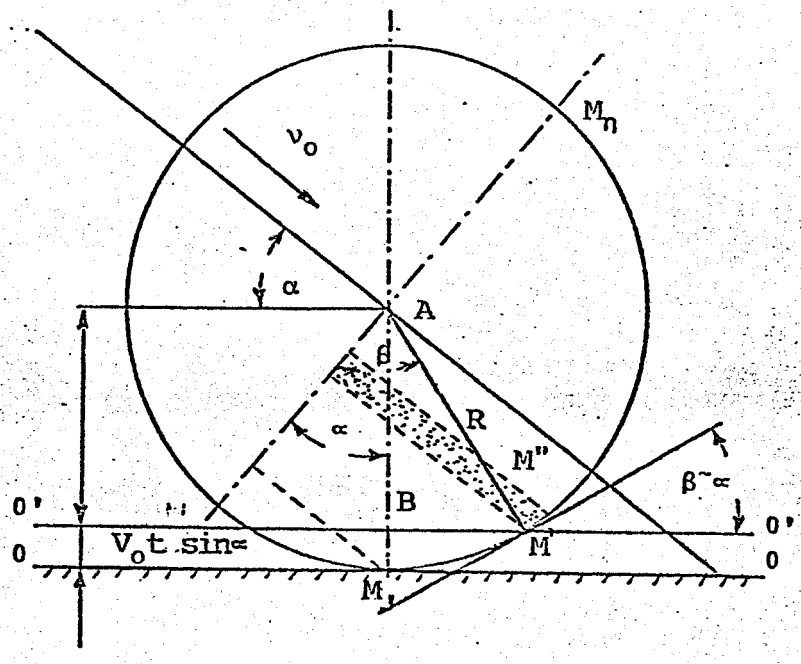

FIG. 7 – Geometric representation of the impact of a bubble with an oblique surface.

impact the contact point moves along radius R to the point M_n. The value of β will vary from α to 180° in the interval

$$0 \leq t \leq \frac{R(1 + \sin \alpha)}{V_o \sin \alpha}$$

and

$$\gamma = 180 - \beta$$

which can be substituted into Eqs 3, 14, 16, and 17 to give a new set of equations valid for the central portion of the droplet,

$$\frac{V_{fj}}{V_o} = \frac{\sin \alpha + \sin \beta}{\sin(\beta-\alpha)} \tag{18}$$

$$\frac{EK_{fj}}{EK_{in}} = \frac{[1 - \cos(\beta-\alpha)] (\sin \alpha + \sin \beta)^2}{2 \sin^2(\beta-\alpha)} \tag{19}$$

$$\frac{K_{fj}}{K_{in}} = \frac{(\sin \alpha + \sin \beta)^2 \sin \alpha}{\sin^3(\beta-\alpha)} \tag{20}$$

Representative values obtained using these equations are shown in Fig. 8, 9, and 10.

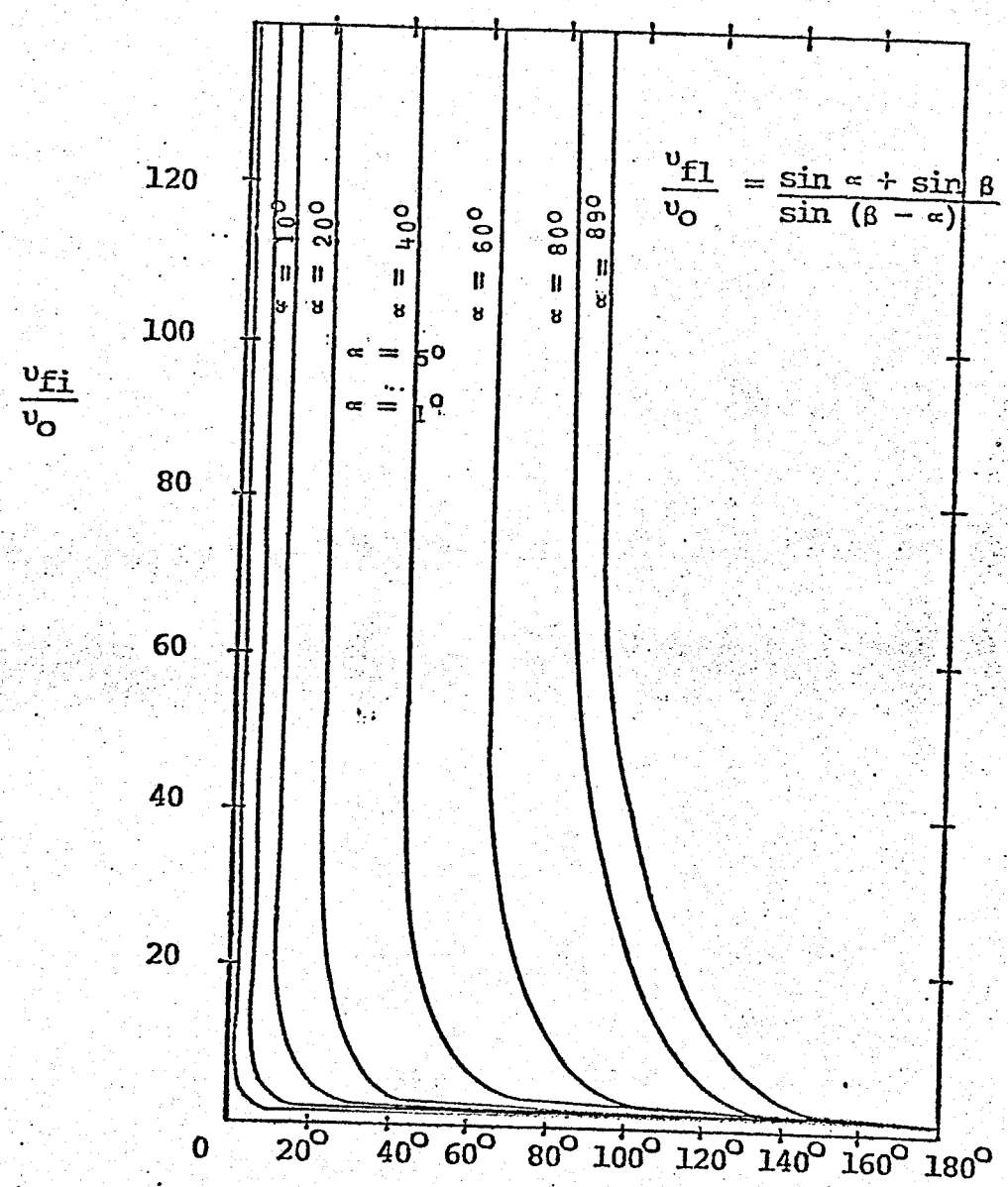

FIG. 8 – Velocity augmentation ratio for a droplet impact as a function of the angles α and β.

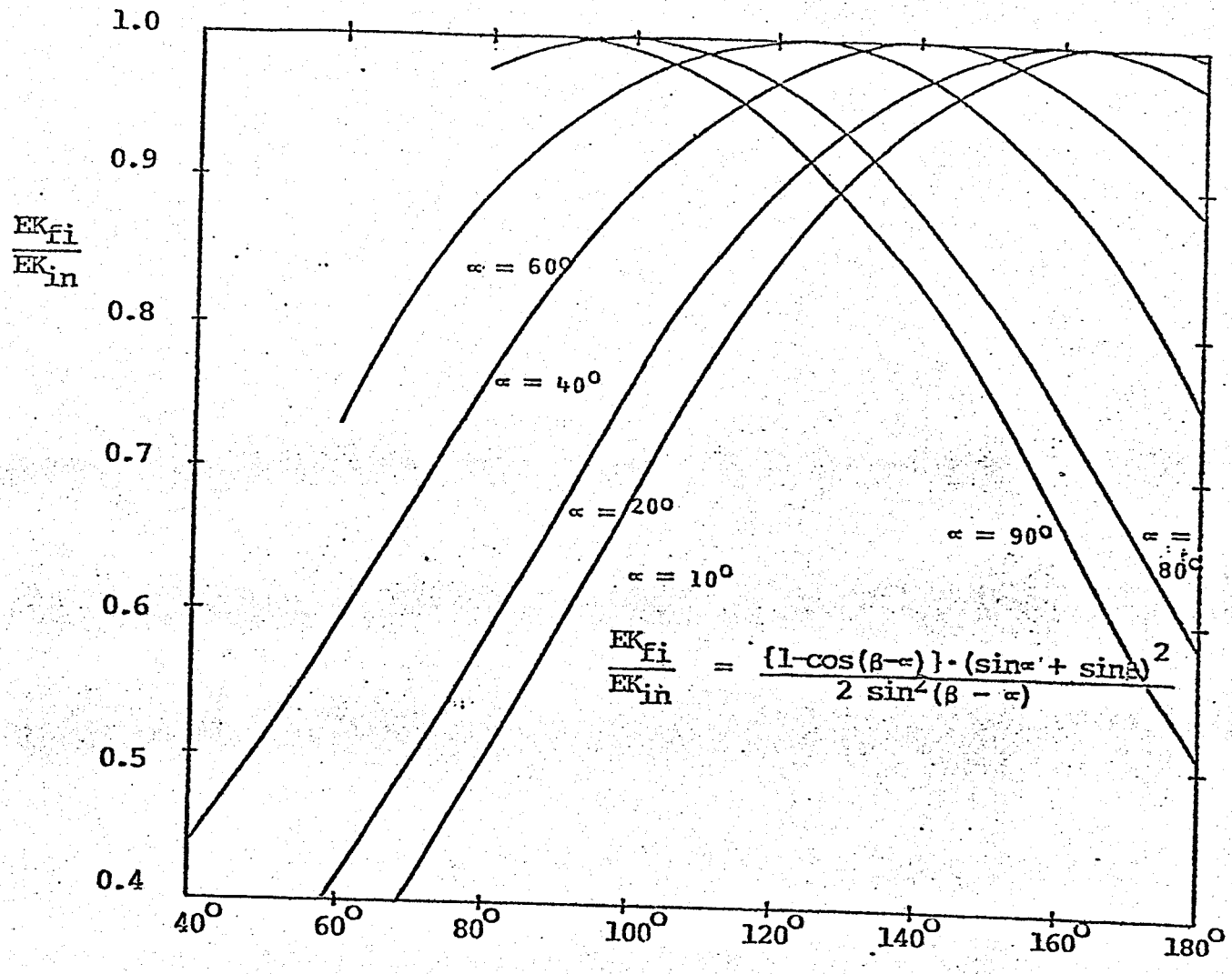

FIG. 9 – Kinetic energy augmentation ratio as a function of the impact angles α and β for a droplet.

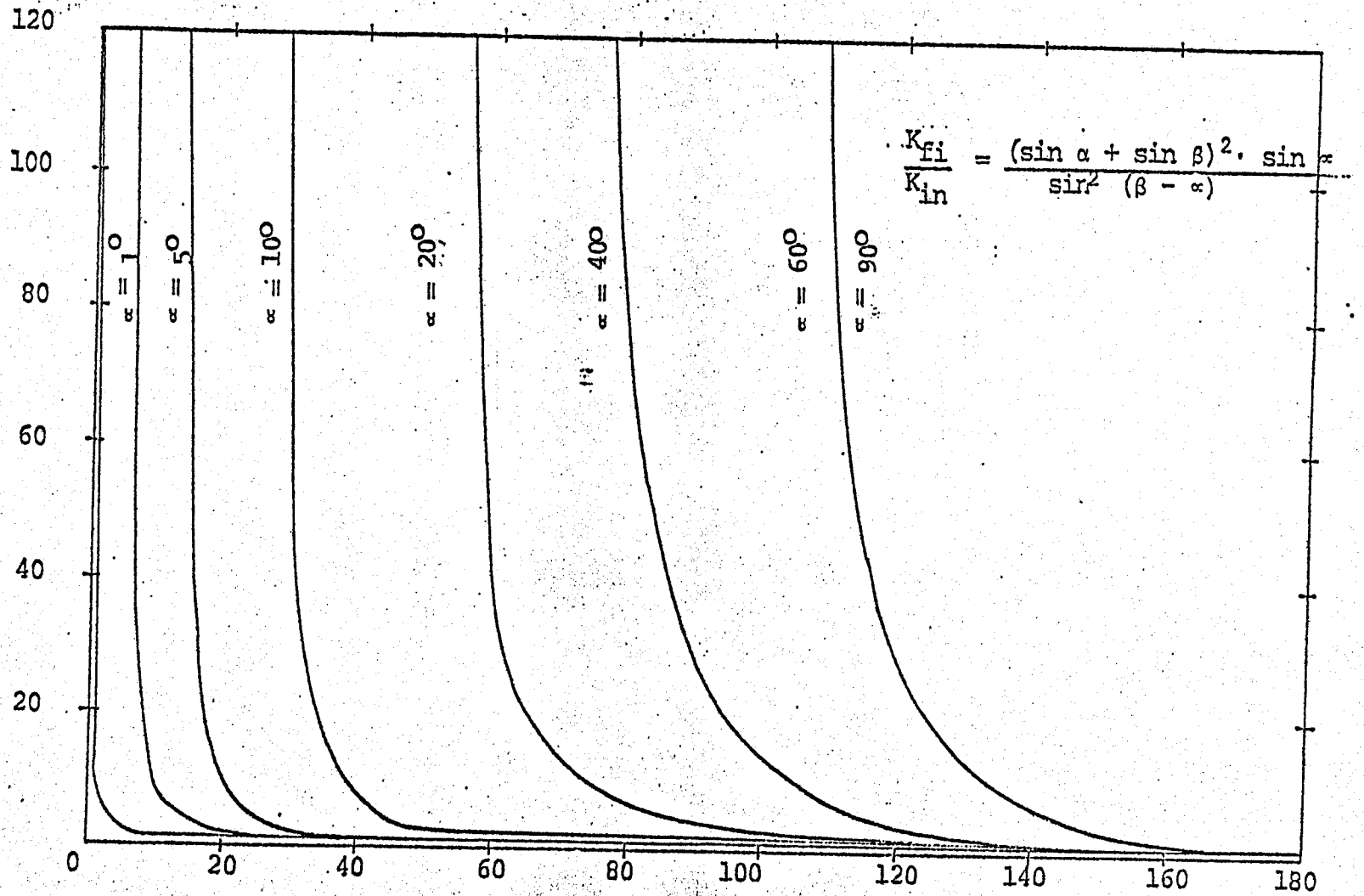

FIG. 10 - Energy intensification ratios as a function of the impact angles α and β for a droplet impact.

Discussion of These Results

The fast jet velocity ratio (Fig. 8) when plotted as a function of the angle indicates that the curves for various values of α are similar in shape but displaced as a function of β. In every case the velocity ratio becomes very large as the angle α approaches the value of β. For practical considerations, the range of β that leads to the formation of satisfactory fast jets is considered to be $\alpha \leq \beta \leq \alpha + 15°$.

From the curves on Fig. 9 which show the kinetic energy ratio as a function of the angles β and α, the same conclusions can be drawn as for the earlier case of a flat impact shown in Fig. 5. The highest energy ratios occur when α and γ are equal ($\gamma = 180 - \beta$).

The concentration of energy ratio shown plotted in Fig. 10 is similar to that for a flat faced jet (Fig. 6). It is again found that as α approaches β so the energy ratio tends to infinity. Where values of α are small the range of β over which the jet energy is highly concentrated is also small, but as α increases so the width of the angle β over which a highly intensified jet is produced is also increased. It is interesting to note that the kinetic energy augmentation is at an optimum where $\alpha = \gamma$ and that the energy intensification is at an optimum where $\alpha = \beta$. Since $\gamma = 180 - \beta$ this suggests that the optimum energy augmentation with the most concentrated jet might occur when $\alpha = \beta = \gamma = 90°$. Under such circumstances the fast jet would be at greatest damage potential when the vertically impacting drop

is at its maximum contact diameter. In this regard investigators at Cambridge [5] have found that damage from impacting droplets is confined to the periphery of the droplet impact zone. The equivalence of the relationship between droplet flow and continuous jet flow is suggested by a corresponding result obtained at Rolla with a high pressure continuous jet directed at an aluminum target located 2.5 cm from the jet nozzle (Fig. 11), where damage is also confined to the region at and beyond the jet impact periphery.

Experiments have, however, concentrated on examining the zone of jet interaction further down the jet stream where the flow has disrupted into droplets. Fig. 12 shows a photograph of such a jet collision with an impact angle of (α) 10° at 4 bar obtained by the strobe flash technique [9]. All the droplet components of each jet do not impact other droplets since there is no control over their spatial distribution and velocity. However, when two droplets do collide, the shock wave generated by the fast jet is clearly visible. The results are similar to those of a collapsing cavitation bubble which produces a Monroe jet with accompanying shock waves [6]. It is similar to the photographs obtained by Edney [7] of the explosive extrusion of the water jet in a vacuum.

In practice the structure of a high pressure water jet, particularly at velocities of the order of 300 m/s, is extremely sensitive to interference from adjacent bodies [8].

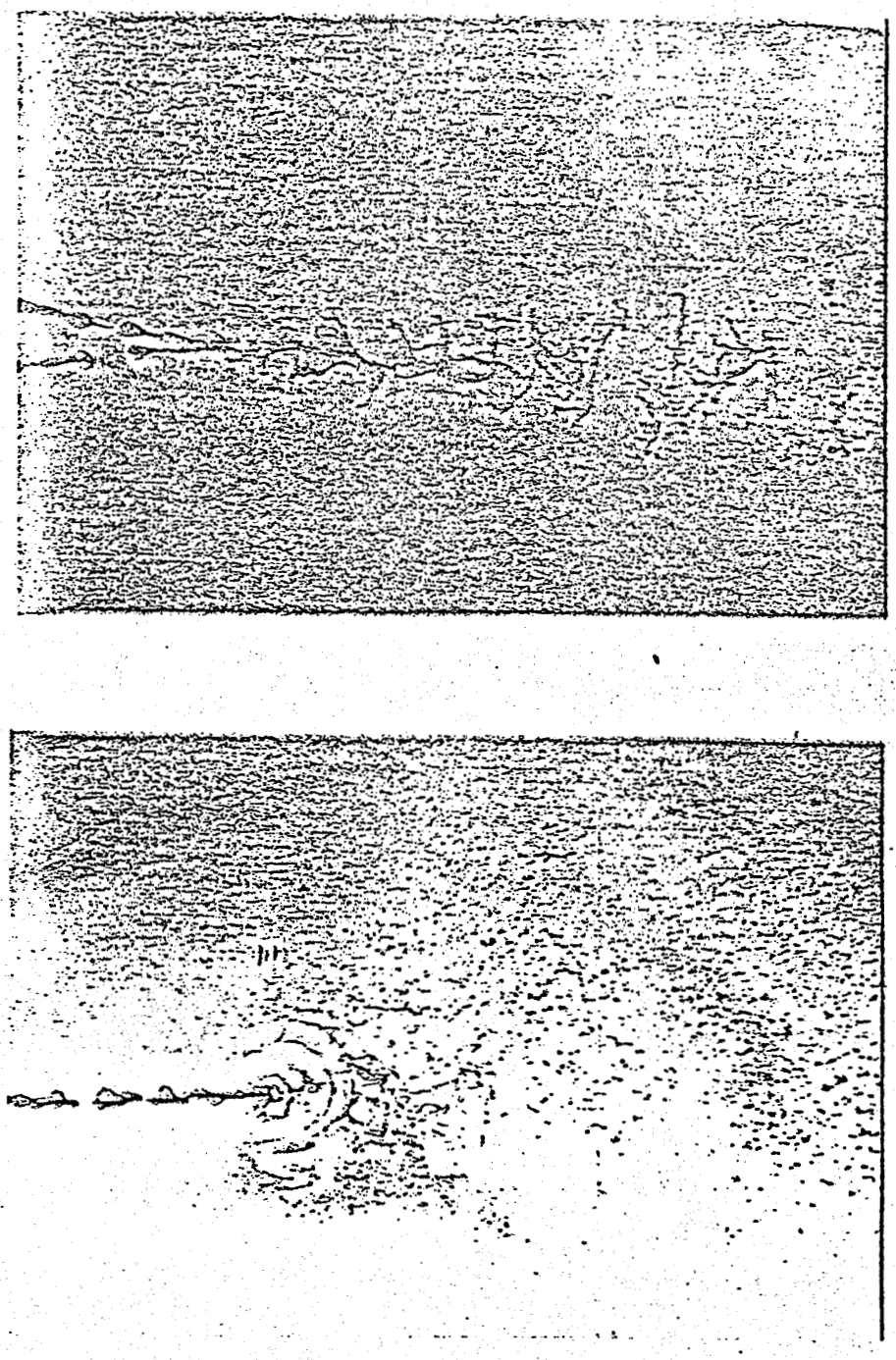

FIG 12- Views of water jets at a pressure of 4 bar converging at an angle of 10° at the point where the jet turns into droplets (a) top view showing the angle of impact, (b) side view showing shock waves generated by the small augmented jet velocity.

For this reason, while water jet impact on solid bodies can be used to generate augmented velocities, the diffuse structure around two continuous jets will interfere with the jet structure prior to impact and negate much of the proposed augmentation. Conversely, once the jet has disintegrated into droplets this is no longer the case, although the target location should be in the immediate vicinity of the impact point since the fast jets produced are extremely small and thus rapidly disrupted. Further research on the effectiveness of interfering jets, designed to interact beyond the jet collapse distance is therefore required.

ROCK CUTTING EXPERIMENTS

As a practical test of the potential effectiveness of converging jets, an experiment was carried out on Berea sandstone samples, 15 cm diameter and 30 cm long, with test nozzles placed 1.25 cm above the sample. The jet pressure was 680 bar for this study in which approximately 20 different nozzle geometries were examined. Nozzles were constructed to produce two parallel jets of diameter 1 mm, separated by distances of 1.27 mm, 1.78 mm, and 3.0 mm. Nozzles were also constructed to produce converging jets at included angles of 1°, 2°, 5°, 10°, 15°, and 20°. All the nozzles were machined from brass and the inside surfaces of the nozzles were lapped.

The best results were obtained with the parallel nozzles with the 1.27 mm and 1.78 mm spacing and the convergent

nozzles with 1° and 2° included angle. The results from the 5°, 10°, 15°, and 20° angle were poor, no cumulative effect being observed. The sandstone samples were split after an exposure time of 10 to 15 s when either the 1° or 2° nozzles were tested (Fig. 13).

Fig. 14 shows one of the convergent nozzles located just above the sandstone. Using the parallel nozzles with 1.27 mm and 1.78 mm spacing gave similar results to those of the 1° and 2° convergent nozzles. One reason postulated for this is the Coanda effect by which two jets flowing close together tend to merge into one jet.

Subsequent to the conclusion of this experiment the authors were engaged in research on a hydraulic mining unit in a surface mine in northern Missouri [8]. The seam of coal was being mined by water jets at a pressure of 680 bar when it was discovered that the coal was interlayered with pyrite lenses, compressive strength of the order of 2,000 bar. Under normal conditions the jets would not cut this material and a set of converging jet nozzles was inserted into the cutting head. The jets produced cut the pyrite satisfactorily allowing the mining machine to advance at a rate of 1.7 m/min.

CONCLUSIONS

The use of external augmentation techniques to improve water jet cutting ability has been demonstrated to be an effective way of improving the cutting of rock and is a means of generating higher pressures than those extant within

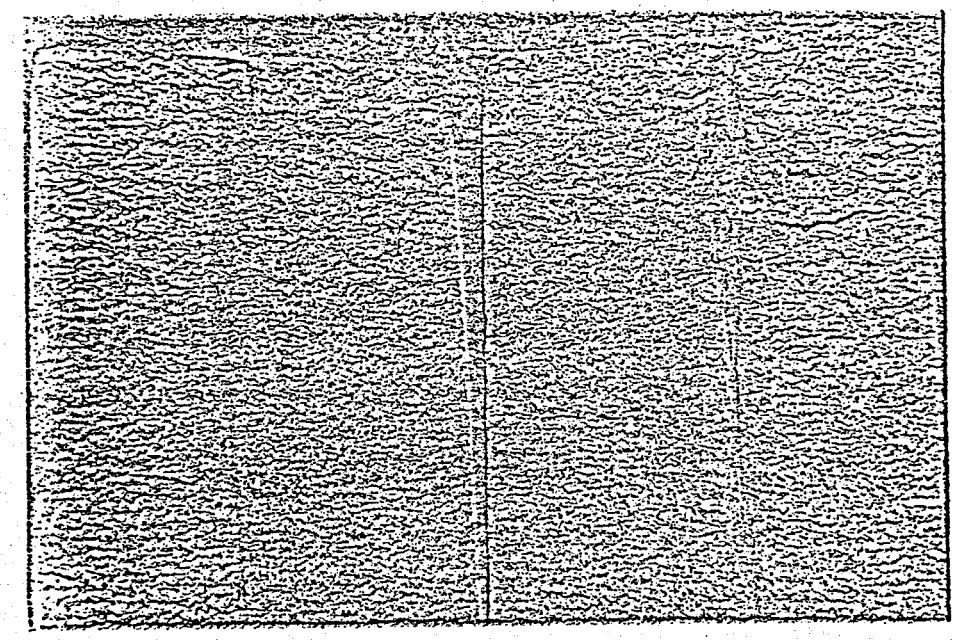

FIG. 13 - Cavity cut into Berea sandstone by a converging jet showing the narrow cut made by secondary jet action.

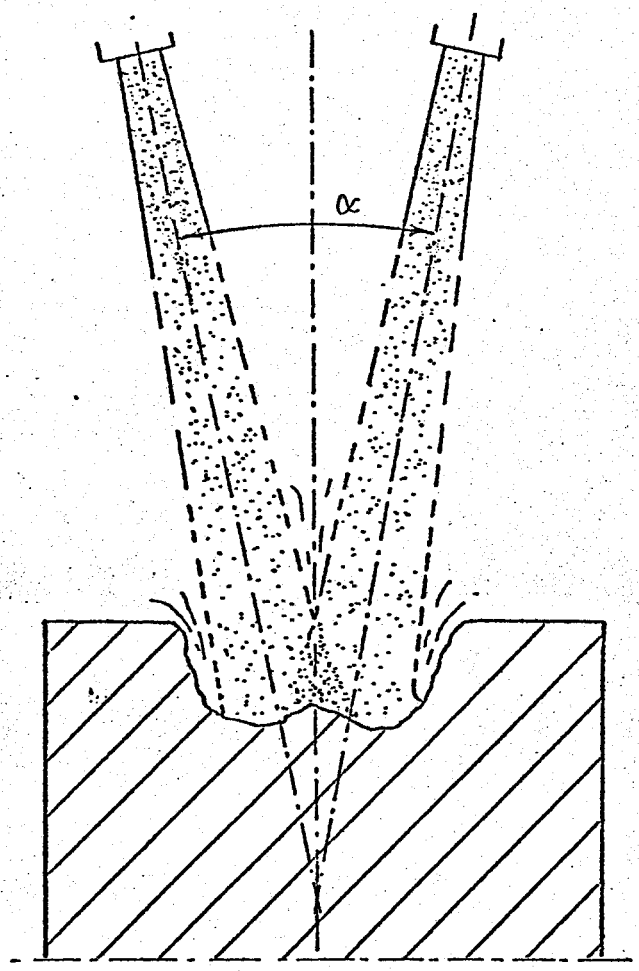

FIG. 14 - Proposed geometry for augmented cutting using the enhanced velocity effects from colliding droplets.

the pre-existing flow. Because of the problems which arise in bringing two flat ended jets together exactly symmetrically, it is proposed herein that a more effective technique would be to converge the jets at a point where they have just broken into droplets. Photographic evidence of such an event shows that large velocity augmentation is possible.

REFERENCES

[1] Birkhoff, G. et al, "Explosives with Lined Cavities," Journal Appl. Phys., Vol. 19, June 1948.

[2] Walsh, T.M. et al, "Limiting Conditions for Jet Formation in High Velocity Collisions," Journal Appl. Phys., Vol. 27, No. 3, March 1953.

[3] Eichelberg, R.J. and E.M. Pugh, "Experimental Verification of the Theory of Jet Formation by Charges with Lined Cavities," Journal Appl. Phys., Vol. 23, No. 5, May 1952.

[4] Bowles Engineering Corporation, "Externally Augmented Hypervelocity Jet Program," Final Report R-10-31-69, Contract DOT-FR-9-0015.

[5] Brunton, J.M., "The Physics of Impact and Deformation Single Impact, (I) High Speed Liquid Impact," Phil. Trans. Roy. Soc., Series A, Vol. 260, pp. 79-85, July 28, 1966.

[6] Summers, D.A. and D.J. Bushnell, "Proceedings of the Workshop on the Application of High Pressure Water Jet Cutting Technology," University of Missouri-Rolla, 1975.

[7] Edney, B.E., "Experimental Studies of Pulsed Water Jets," 3rd International Symposium on Jet Cutting Technology, Chicago, May 1976.

[8] Summers, D.A., C.R. Barker, and M. Mazurkiewicz, "Development of a Longwall Water Jet Mining Machine," Phase III Report, University of Missouri-Rolla, 1977.

[9] Summers, D.A. and J.L. Zakin, "The Structure of High Speed, Fluid Jets and Their Use in Cutting Various Soil and Material Types," Final Report on USA MERDC Contract DAAK 02-74-C-0006, April 30, 1975.